Improvement of the self-assembly of low χ ABA triblock copolymers with the addition of an ionic liquid

Aynur Guliyeva,[†] Hélène Pung,[†] Sylvie Tencé-Girault,[†, ‡] Marc Rébillat,[†] Anatoli Serghei,[#] Matthieu Gervais,[†] Cyrille Sollogoub,[†] and Sébastien Roland[*,†]

[†]Laboratoire PIMM, Arts et Métiers Institute of Technology, CNRS, Cnam, HESAM Université,75013 Paris, France

[‡] Arkema, CERDATO, 27470 Serquigny, France

[#] Laboratoire Ingénierie des Matériaux Polymères, UMR CNRS 5223, Université Lyon 1, 69621 Villeurbanne, France

[*]Correspondance to: Sébastien Roland (email: sebastien.roland@ensam.eu)

ABSTRACT: Self-assembly of high molecular weight commercially available low χ ABA triblock copolymers with ionic liquids was observed after solvent casting without the implementation of an additional annealing step. Here, the addition of an ionic liquid (IL) to a triblock copolymer poly(methyl methacrylate-b-butyl acrylate-b-methyl methacrylate) (MAM) with an elastomeric central block and rigid end blocks is proposed to tune the self-assembled morphology. Two different compositions of this copolymer with different initial microstructures (ill-defined morphology without long-range order and a lamellar morphology) were selected. The selectivity of the IL addition in one of the block phases was studied through the evolution of the glass transition of both blocks. The impact of the IL weight concentration on the morphology as well as the domain spacing was presented. Adding IL to the first copolymer detected a lyotropic disorder-order transition towards a gyroid morphology, observed even for a high molecular weight copolymer due to the low χ parameter and for higher IL content a second transition to a lamellar morphology was observed. For the second one, only an order-order transition (lamellae to cylinders) could be detected at high IL content. IL also enhanced the long-range ordering of the MAM morphology obtained through solvent casting without additional annealing steps, compared to the same composition without IL.

Introduction

Block copolymers (BCPs) show well-ordered nanostructures with dimensions ranging from 5 nm to as large as 100 nm, which are obtained by two or more immiscible and covalently linked polymer blocks having different chemistries. They are promising to develop new functional materials for various applications from nanoporous membranes to nanoelectronic devices.[1–7] Controlling the BCP morphologies through chemical, physical, or processing ways remains a challenge and is still a hot topic discussed in the literature.[8,9]

To avoid complex synthesis methods, well-known industrial-scale produced block copolymers (thermoplastic elastomers A-B-A) attract particular attention as good candidates, both for research studies and applications. However, the limited choice among these polymers reduces the targeted-sized morphologies. Thus, the modification of preexisting industrial block copolymers by methods other than chemical (melt processing,[10] solvent processing selectivity,[11–13] solvent evaporation rate[14] or additives[15–22]…) can be a solution to produce new materials with different parameters without challenging steps. Blends of BCPs with functional additives have proven to be increasingly interesting since adding small molecules gives new compelling properties to the preexisting BCPs without the implementation of complex syntheses and provides a versatile method for fabricating predictably ordered microstructures.

More recently, ionic liquids (ILs) have emerged as a class of chemicals which are room-temperature molten salts composed entirely of ions.[23,24] They show unique properties such as high thermal and chemical stability, non-inflammability, negligible vapor pressure, very low toxicity, and high ionic conductivity.[25,26] ILs become great candidates for the creation of functional materials due to their tunable properties such as hydrophilicity, acidity, and hydrogen bonding because of the unlimited possibilities for anions and cations combinations. These

properties make them highly compatible with various synthetic polymers and good candidates as solvents or additives.[27–29]

In the literature, several diblock copolymers, such as poly(styrene-*b*-ethylene oxide) (PS-*b*-PEO),[30] poly(styrene-*b*-methyl methacrylate) (PS-*b*-PMMA),[31–33] poly(styrene sulfonate-*b*-methyl butylene) (PSS-*b*-PMB)[34,35] or poly(styrene-*b*-2-vinyl pyridine) (PS-*b*-P2VP),[36–38] have been blended with ILs which appear to be miscible with the more polar block of the copolymer. For instance, for PS-*b*-PMMA, certain ILs have been found to preferentially associate with the polar PMMA block of copolymer.[31–33] The ILs act as plasticizers as they enhance the mobility of this block, reducing the glass transition temperature. Interestingly, they also increase the Flory-Huggins interaction parameter χ and influence the center-to-center distance by swelling the IL-containing phase.[31–33,37,39,40] Order-to-order lyotropic morphology transitions from lamellar to disordered spherical have been observed by studying different ILs and changing their relative amount in a same BCP.[31–33]

Materials based on ILs and BCPs have already found applications in several areas, such as in the manufacturing of polymer electrolytes for batteries, membranes, fuel cells, actuators, and photonics.[34,41–44] The common denominator in all these applications is the need to produce a material that is not only conductive but also solid, which are two antagonistic properties for this type of materials. Indeed, the ionic conductivity is necessarily associated with molecular mobility, which *de facto* reduces the mechanical properties of the final material. Then, the use of ABA triblock copolymers, ensuring both mechanical strength and ionic conductivity, appears obvious. By selectively incorporating ILs within nanostructured morphologies of triblock copolymers, the best of both worlds could be achieved. Watanabe et al. investigated the microstructures, rheological properties, and ionic conductivity of ionic gels formed by self-assembly of PS-*b*-PMMA-*b*-PS triblock copolymers with 1-ethyl-3-methylimidazolium bis(trifluoromethyl-sulfonyl)imide ([Emim][Tf2N]).[45] PS, immiscible with IL, creates

spherical domains that serve as physical crosslink points. PMMA forms the continuous phase with the IL, which serves as the ionic conduction path. These polymer electrolytes were then used as an electroactive polymer actuator composed of ion gel electrolytes sandwiched between two composite carbon electrodes. By applying low voltages (<3.0 V) to the electrodes, the actuator exhibited a slow bending motion towards the anode side. The IL concentration and the length of the actuator (geometry of materials) have effects on the movement of the actuator. Various studies have confirmed the observation of greater displacement of the actuator by increasing the concentration of IL in the material and/or the length of the actuator.[45] The ionic conductivity measurements on these materials confirmed the relation between tortuosity of different morphologies and ionic conduction path, which is crucial for the application.[46,47] But the effects of ILs to obtain different possible morphologies for self-assembly and the effects of different types of morphologies on mechanical strength and ionic conductivity of the final material remain as a challenging question in the literature. For this, the gyroid morphology is targeted as it allows cocontinuous nanostructures leading to high ionic conductivity. In classical BCP systems, N is usually decreased to obtain low χN values close to the Weak Segregation Limit, in which the gyroid morphology is present. However, in this region, small molecular weights lead to low mechanical properties, which limits their practical use.

In this work, we used a BCP with high molecular weight and low χ parameter to access the Weak Segregation Limit in the vicinity of the order-disorder transition. The objective was to promote the gyroid morphology by adding an ionic liquid. Thus, we studied the effect of ionic liquids additives on the self-assembly process of ABA type triblock copolymers with an elastomeric central B block and rigid end A blocks which are well-known commercially available thermoplastic elastomers (TPEs), namely poly(methyl methacrylate-*b*-butyl acrylate-*b*-methyl methacrylate) (MAM). The two blocks have chemical similarities that provide a very low χ parameter ($\chi_{PMMA/PBUA} = 0.047$).[48,49] Two different compositions of the same copolymer

(MAM M52 with lamellar morphology and MAM M53 in the with ill-defined morphology without long-range order) were tested to study the impact of IL on the structuration (from disorder to ordered state) and improvement of the existing morphologies (from ordered state to well-ordered morphology) of BCPs. The MAM polymer films with and without ILs additives were characterized by different techniques to analyze their final morphologies. The IL content in the BCP was varied to enhance the formation of well-ordered morphologies in solvent-cast films.

Experimental section

Materials. Poly(methyl methacrylate-*b*-butyl acrylate-*b*-methyl methacrylate) (PMMA-PBuA-PMMA, MAM) under the reference M52 and M53 triblock copolymers were supplied by ARKEMA from their Nanostrength® trademark and used without any further purification. Polymer molar masses were determined by SEC at 40 °C using THF as eluent on a Waters apparatus equipped with three columns Styragel HR0.5, HR3 and HR4 and with a Waters 2414 refractive index detector at an elution rate of 1 mL/min (**Table 1**). Polystyrene was used as standards. 1-ethyl-4-methylpyridinium bis(trifluoromethyl-sulfonyl)imide ([4empy] [Tf2N]) ionic liquid (T_m = 5 °C; T_g = -53 °C) was purchased from Iolitec GmbH and heated under vacuum at 50 °C for a few hours prior to use to remove any remaining moisture.

NMR spectroscopy. 1H (400 MHz) NMR measurements of the triblock copolymers M52 and M53 were performed on a Brüker Avance 400 spectrometer, in CDCl$_3$ at room temperature in order to determine their composition.

Table 1. MAM M52 and MAM M53 molar masses and composition (f_{PMMA} and f_{PBuA} − volume fraction of PMMA and PBuA block respectively) (see on Fig.S1 and S2 in Supporting Information)

Copolymer	M_n (kDa)	M_w (kDa)	Dispersity $Đ$	f_{PMMA}	f_{PBuA}
MAM M53	77.9	132.0	1.70	46	54
MAM M52	99.6	203.8	2.05	70	30

Solvent Cast. Bulk samples, *ca.* 500 µm thick, were obtained by slow evaporation of 200 mg/mL concentration of the BCPs solutions with IL in chloroform ($CHCl_3$) overnight and then dried under vacuum at room temperature for 6 hours.

Differential Scanning Calorimetry (DSC). Differential scanning calorimetry measurements were performed using a TA Instruments DSC Q10 calibrated beforehand with an indium standard scanned at 15 °C/min. All the samples (~ 10 mg) were heated from -80 °C to 200 °C at a heating rate of 15 °C/min under nitrogen flow (50 mL/min). Data from the second heating cycle were used to determine the glass transition temperature (T_g).

Atomic Force Microscopy (AFM). AFM phase images were obtained using tapping mode of a Multimode V.8 microscope driven by a Nanoscope V controller (Bruker) with silicon tips (spring constant 40 N/m, oscillation frequency 300 kHz) purchased from Budget Sensors. Sample surfaces were prepared using a diamond knife on an LKB BROMMA 2088 ultramicrotome at room temperature and on ultramicrotome Leica EM FC6 at -70°C. To improve the cutting step at room temperature, prior to triblock copolymers microtomy, mixtures of BCPs with ILs were immersed in a 10 wt% aqueous solution of phosphotungstic acid (H_3PO_4-$12WO_3$, denoted PTA) over 19 hours to react with and harden the PBuA phase.[51]

Small-Angle X-ray Scattering (SAXS). SAXS studies were carried out using the high-brilliance SWING beam line at the Soleil Synchrotron facility, with a monochromator set at 16 keV leading to a wavelength of 0.77 Å. Scattering patterns were recorded using a CCD detector at 400 cm from the sample. 500 µm thick films were put on a sample holder. 10 2D SAXS

patterns were recorded with acquisition time set to 250 ms. 1D SAXS patterns curves were obtained by circular averaging of the 2D images using the Foxtrot software. A Nano-inXider SW (Xenocs) system, equipped with a microsource GeniX3D (λ = 1.54 Å) and a detector Pilatus3 (Dectris), was also used for complementary experiments. Scattering patterns were recorded during 600 s. Normalized and corrected 1D spectra were obtained using Foxtrot software.

Results and discussion

1. Ionic Liquids and Block Copolymers Miscibility. The selectivity of ILs with BCPs is of critical importance to understand the blends nanostructuration. The miscibility of the small molecule in one of the blocks of the copolymer is usually detected by glass transition temperature (T_g) shifts.[31,40,52] DSC is then the method of choice to study the impact of the presence of ILs on T_g. The heat flow thermograms of MAM block copolymers M52 and M53 with increasing ILs weight concentrations are shown in Figure 1. At the studied concentrations, the IL seems to be fully dispersed in the BCP matrix as no melting peak was observed at *ca.* 20 °C (see on Fig.S3 in Supporting Information). The T_g of the PMMA block for the pure M53 BCPs is equal to 117 °C (glassy at room temperature), whereas the T_g of the PBuA block is *ca.* -40 °C (rubbery at room temperature). Adding IL to the BCP causes a significant drop in the T_g of the PMMA block, decreasing to 2 °C with φ_{IL}= 44 wt%. The T_g of the PMMA block of the M52 BCP is 124 °C decreasing to *ca.* 50 °C at the highest IL content (44 wt%). Both insets in Figure 1 show the evolution of the T_g of the PMMA block as a function of IL content. It shows a monotonous decrease, which follows the blend rule. At the same time, the T_g of the PBuA block remains fairly stable (rubbery at room temperature) for all IL concentrations, even though a very small shift towards lower temperatures can be observed at higher IL concentrations for MAM M53.
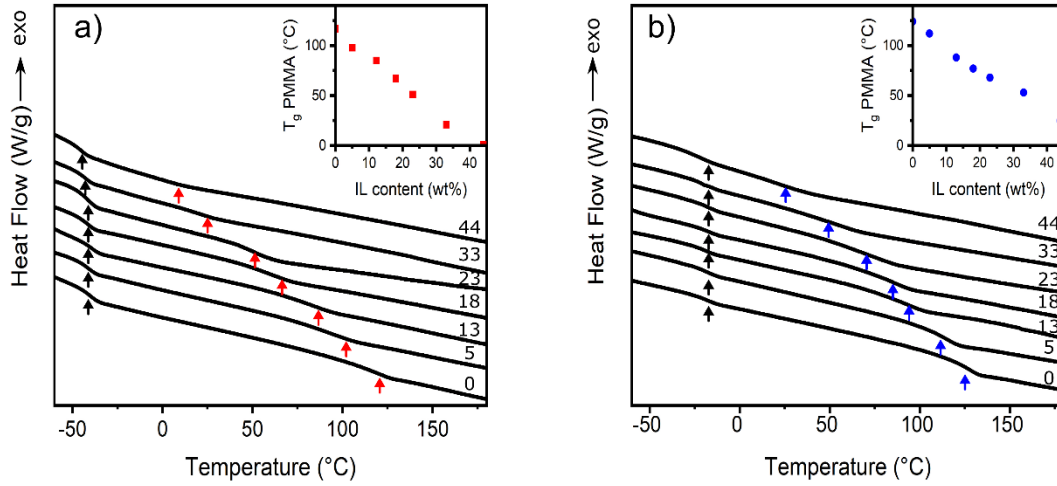
Figure 1. DSC curves for MAM M53 (a) and MAM M52 (b) block copolymers blended with ionic liquid (IL) over different weight concentrations (φ_{IL}): 0%, 5%, 13%, 18%, 23%, 33%, and 44%. The arrows indicate the T_gs of the PBuA block (black) and the T_gs of the PMMA block (red for M53 and blue for M52). Insets show the evolution of the T_g of the PMMA block as a function of IL content (wt%).

Since it appears that the IL only dissolves in the PMMA phase, the IL content (φ_{IL}) in Figure 1 can be corrected in absolute concentration in PMMA (φ_{IL}^{corr}), knowing the PMMA content in each BCP. The following formula can then be used:

$$\varphi_{IL}^{corr} = \varphi_{IL} \times w_{PMMA} \qquad \text{(Eq. 1)}$$

With w_{PMMA} the weight fraction of PMMA in the BCP.

The evolution of the T_g of the PMMA phase can then be plotted as a function of φ_{IL}^{corr}. The data are shown in Figure 2. In both BCP, this evolution confirms that the IL acts as a plasticizer in the PMMA phase, to the same extent, regardless of the block copolymer. The evolution follows the blends rule leading to an extrapolated T_g of the IL at *ca.* -55 °C, which is close to the value measured in DSC (-53 °C). This shows that the IL is entirely incorporated in the PMMA phase and excluded from the PBuA phase for the studied concentrations.
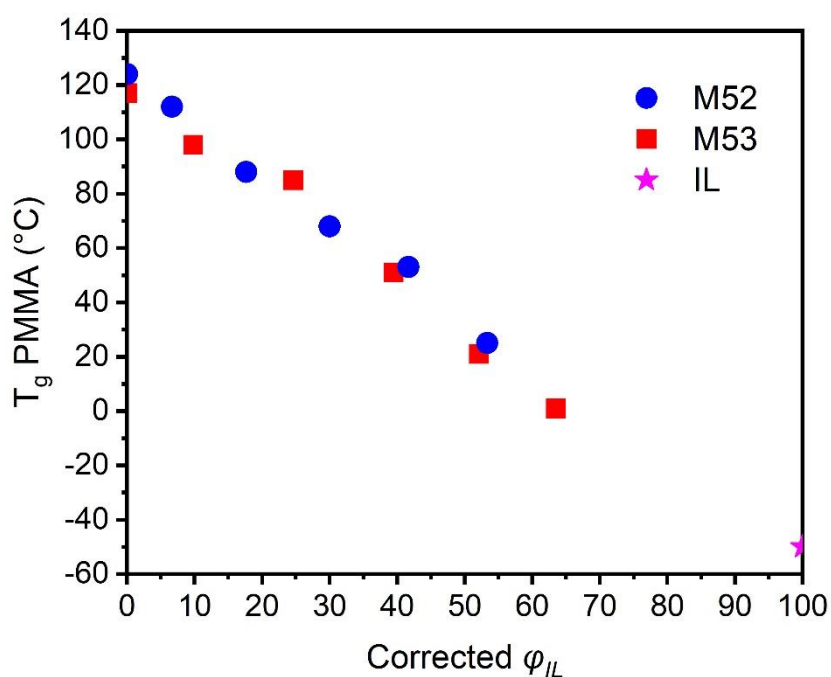
Figure 2. T_g of the PMMA block corrected with the ionic liquid content in the PMMA phase for the M52 (●) and the M53 (■) BCPs. The T_g of the ionic liquid (★) is also shown.

The strong selectivity with the PMMA phase and its immiscibility with the PBuA phase can be explained by the presence of van der Waals interactions between ILs (highly polar) and PMMA chains (polarity higher than PBuA chains). This behavior has been observed for PS-PMMA copolymer/IL blends where the IL was preferentially and totally solubilized in the PMMA nanophases, the PS phase being less polar.[31,40] Due to the slight difference in the chemical structure of the repetitive unit of MAM BCP, a selective incorporation of IL in PMMA block was observed for the studied contents.

2. Effects of Ionic Liquid Addition on MAM M53 and MAM M52 Block Copolymer Bulk Nanostructure.

The prediction of the blend morphologies is an important step towards controlling the ions migration in the material. **Figure 3** displays AFM phase images of the morphological evolution of M53 BCP with different weight concentrations φ_{IL}.

Without IL addition, the BCP is in the disordered state as no specific morphology can be observed. During the evaporation of the non-selective solvent, the blocks of the copolymer are not highly repulsive so that they stay in the disordered state as the concentration of CHCl$_3$ decreases to the point where no further mobility can be reached. The addition of IL in the initial BCP solution induces a gradual disorder-order transition (DOT) from a disordered state to an ordered morphology between 0 and 33 wt%. At an IL concentration of 5 wt%, small ordered domains are seen by AFM, but most of the sample seems to remain in the disordered state, as also observed theoretically by Nakamura et al. and experimentally by several authors, in the case of BCP in the presence of Lithium salts.[53,54] As the IL concentration increases up to 13 wt%, larger ordered domains are detected. It is noteworthy that it is difficult to assign a specific morphology as both dots and stripes are seen by AFM. At an IL concentration of 18 wt% and 23 wt%, a coexistence of two different morphologies and a transition between dots and stripes were observed on AFM images. This suggests a transition from gyroid to lamellar morphology according to the composition of PMMA and PBuA blocks in BCP and the swelling of PMMA induced by the selective incorporation of IL.[31,32] However, it is important to analyze these films by another method to confirm the exact morphologies. As for the 33 wt% morphology, only stripes are observed, which favors the assumption of a lamellar morphology. This last AFM image also shows that the domain size in which a uniformly oriented morphology is observed, increases compared to the samples containing less IL. The 44 wt% sample could not be

observed by AFM due to the plasticizing effect induced by the presence of IL, which prevented us from preparing the surface through ultramicrotomy.
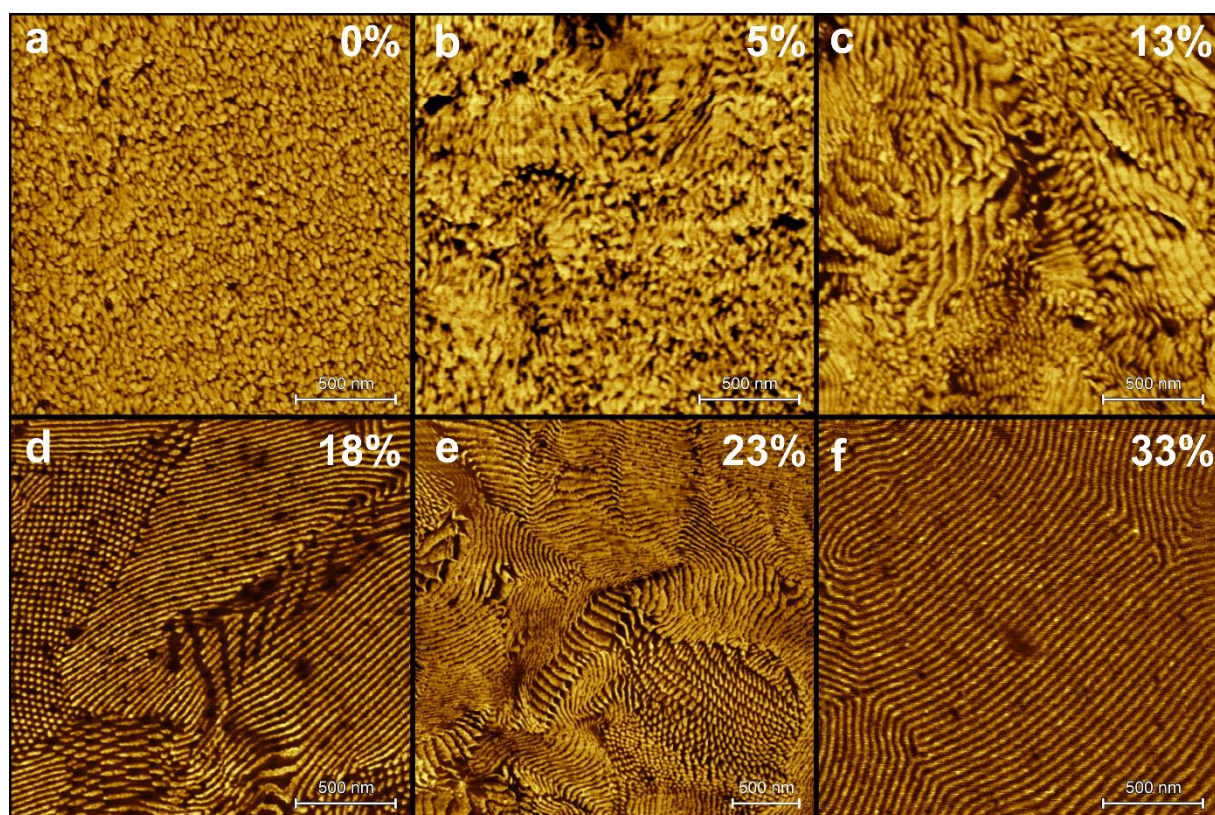

Figure 3. AFM phase images for MAM M53 block copolymer blended with ionic liquids (ILs) with different weight concentrations φ_{IL}: (a) 0%, (b) 5%, (c) 13%, (d) 18%, (e) 23%, and (f) 33%.

Figure 4 shows the morphology evolution of BCP M52. Contrary to M53, without IL, M52 already shows a structured morphology, which can be identified as lamellar. Even though the χ parameter between the two blocks is expected to be low, the difference in molecular weight between M52 and M53 leads to different χN. Therefore, a segregation between the blocks can be seen for pure M52. After the evaporation from a CHCl$_3$ solution, the resulting morphology shows disordered lamellae with tortuous interfaces. The potential impact of dispersity on the block copolymer phase separation behavior should also be highlighted and could explain the observation of deformation of the phase diagram, namely lamellar morphology for MAM M52 without IL. It has been shown that dispersity could cause the swelling of domains and affect the

increase of microdomain spacings in the ordered state, shift the phase boundaries towards larger φ (the order-order transitions (OOTs) to the higher volume fraction of dispersed block), and decrease the critical degree of segregation (χN) for microphase separation, increasing the incompatibility compared to monodisperse copolymers of equivalent $\overline{M_n}$.[55–59] The dispersity in BCP can shift or deform stability region of the various morphologies on the diagram phase. The mechanism of the morphological transition is explained by the competition between interfacial and entropic energies. For disperse systems, the chains with larger dispersity stretch more than those with smaller dispersity even though the blocks have equal compositions. For asymmetric polymer distributions, dispersity favors structures with curved interfaces. The imbalance of stretching energy between opposing blocks curves the interface concave toward the component with the lower dispersity to alleviate the imbalance and relax the stretching energy of the disperse component.[60–63] Because of the deformation of the phase diagram due to the dispersity, the morphology of M52 is therefore not cylindrical. Significant tortuosity of the interfaces for this morphology can probably be explained by the dispersity of the polymer chains at the interface, which causes curved interfaces in order to respond to the balance of stretching energies.

As the IL content increases up to 23 wt%, the block copolymer interfaces must be shortened by the presence of the IL, due to the increasing χ parameter, which leads to larger grains with higher long-range order. At an IL content of 33 wt%, some dots can be observed in minor zones of the AFM image (on Fig.4e', 4f' and g'), which suggests that a transition towards a cylindrical morphology can be suspected, due to a selective swelling of the PMMA phase. This is confirmed by increasing the IL content to 38 wt% and then to 44 wt%. At this concentration, these cylindrical areas widen to the extent of the lamellar areas, leading to a mixed morphology. It seems that no gyroid morphology is detected during this lamellar to

cylindrical transition, probably because of the initial higher molecular weight of the MAM M52 compared to M53.

For both BCPs, at high IL content, larger grain sizes are obtained after solvent evaporation and can be attributed by the presence of stiffer interfaces during the evaporation of $CHCl_3$. For a pure copolymer, as the neutral solvent evaporates, the chains have less and less mobility and a morphology, mainly dictated by the composition of the copolymer, stabilizes. The difference in morphology (non-specific morphology and lamellar) between the two BCPs without IL only comes from the difference in molar mass N, considering a constant χ of the system. When the IL is present in the film, the system has a different χ_{eff}, which increases with the amount of IL.[32] During the evaporation of the solvent, χ_{eff} being larger, one can imagine that the morphology of the mixture is revealed earlier during the evaporation of the $CHCl_3$ and that the domains with stiffer interfaces but also more mobility can then coalesce into larger grains. In addition to the increase in the χ parameter, the IL might add a plasticizing effect at the very end of the evaporation of the solvent molecules. These effects are more pronounced as the IL content is high. However, this impact seems to be limited since at very high IL content (especially for M52), the grain size no longer increases. Nevertheless, since no additional thermal or solvent annealing was used, ILs seem to be perfect candidates to enhance this long-range order.
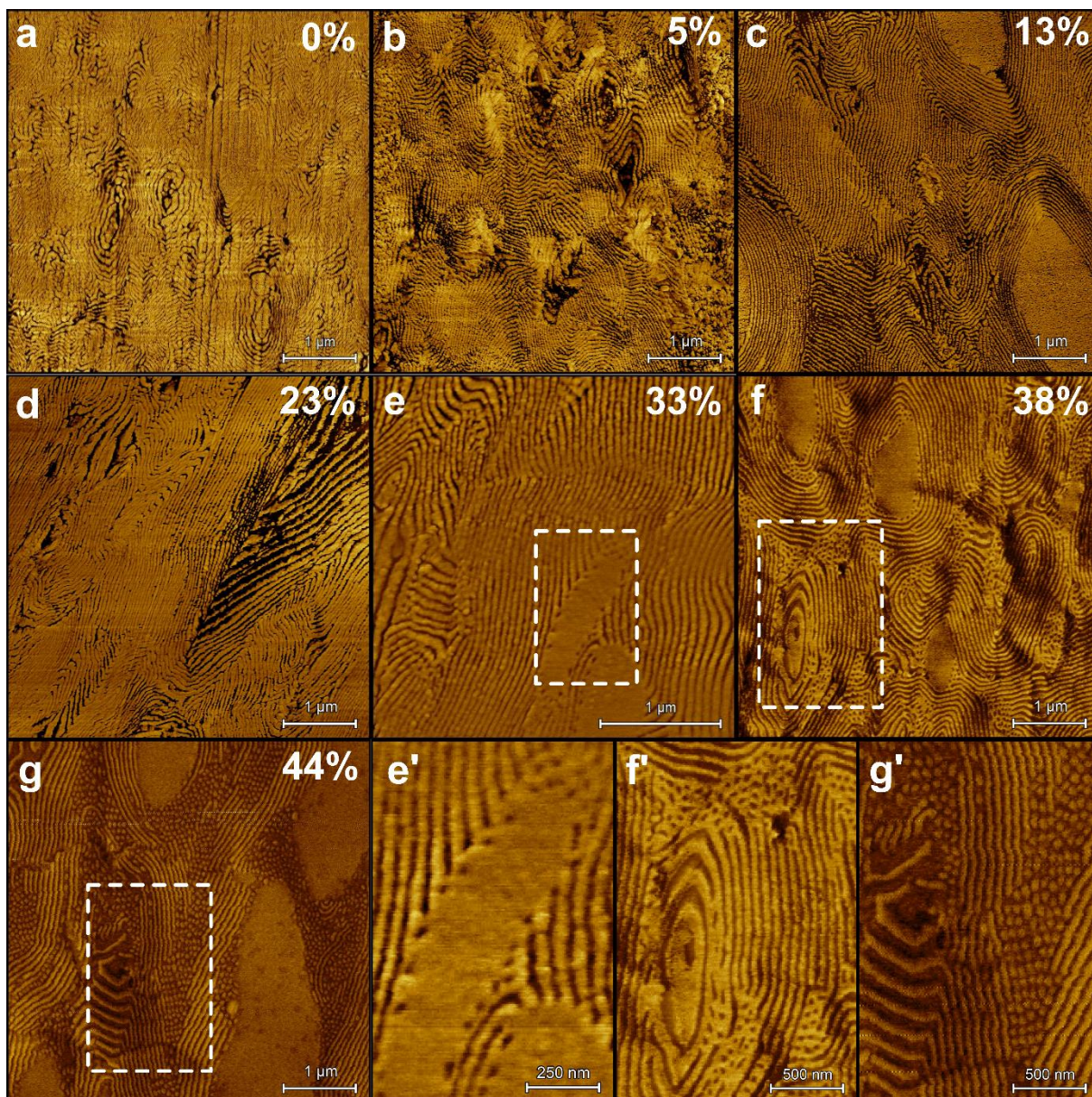
Figure 4. AFM phase images for MAM M52 block copolymer blended with ionic liquids (ILs) over different weight concentrations φ_{IL}: (a) 0%, (b) 5%, (c) 13%, (d) 23%, (e) 33%, (f) 38%, and (g) 44%. (e'), (f'), and (g') are zoomed images of the squared areas in images (e), (f), and (g), respectively.

In **Figure 5**, SAXS 1D profiles of several samples consisted of BCPs mixed with different IL weight concentrations φ_{IL} are shown. **Figure 5a** shows SAXS analysis results for MAM M53 where the morphology of the initial film without IL and of the samples with low IL concentrations (below 13 wt%) can be attributed to an ill-defined morphology with broad peaks, in good agreement with the AFM observations. However, increasing the concentration of IL in the BCP significantly narrows the width of the q* peak and at higher concentrations, higher

order Bragg peaks appear, which is consistent with ordering of the BCP morphology. SAXS patterns of MAM M53 films with 13 wt% and 23 wt% of IL reveal several positions of higher order scattering peaks, especially at $\sqrt{(4/3)}q^*$, $\sqrt{(10/3)}q^*$, $\sqrt{(11/3)}q^*$, $2q^*$, $3q^*$, which can be attributed to a coexisting gyroid/lamellae morphology.[31–33] This result is in good agreement with the AFM images presented in Figure 3c-e showing a coexistence of dots and lines. Lamellar morphology was also confirmed for the MAM M53 samples with higher IL concentration (33 wt% and 44 wt%) by the appearance of numerous higher order peaks at $2q^*$, $3q^*$, and $4q^*$. **Figure 5b** shows SAXS 1D profiles for MAM M52 blended with different IL contents. The initial film without IL and the samples with low IL contents (below 23 wt%) can be attributed to a lamellar morphology. Increasing φ_{IL} reveals higher diffraction orders of the lamellae reaching a maximum of six diffraction orders at 33 wt%. These results further confirm the AFM observations. For MAM M52 with 44 wt% IL, SAXS pattern shows peak positions at $\sqrt{3}q^*$, $2q^*$, $\sqrt{7}q^*$, $3q^*$, $\sqrt{12}q^*$, and $4q^*$. The peaks, which are attributed to a cylindrical morphology, are less pronounced on the SAXS pattern compared to that of the lamellar morphology. Increasing φ_{IL} to 44 wt% caused the transition from lamellae to cylinder nanostructures, which is also in good agreement with the AFM observations.
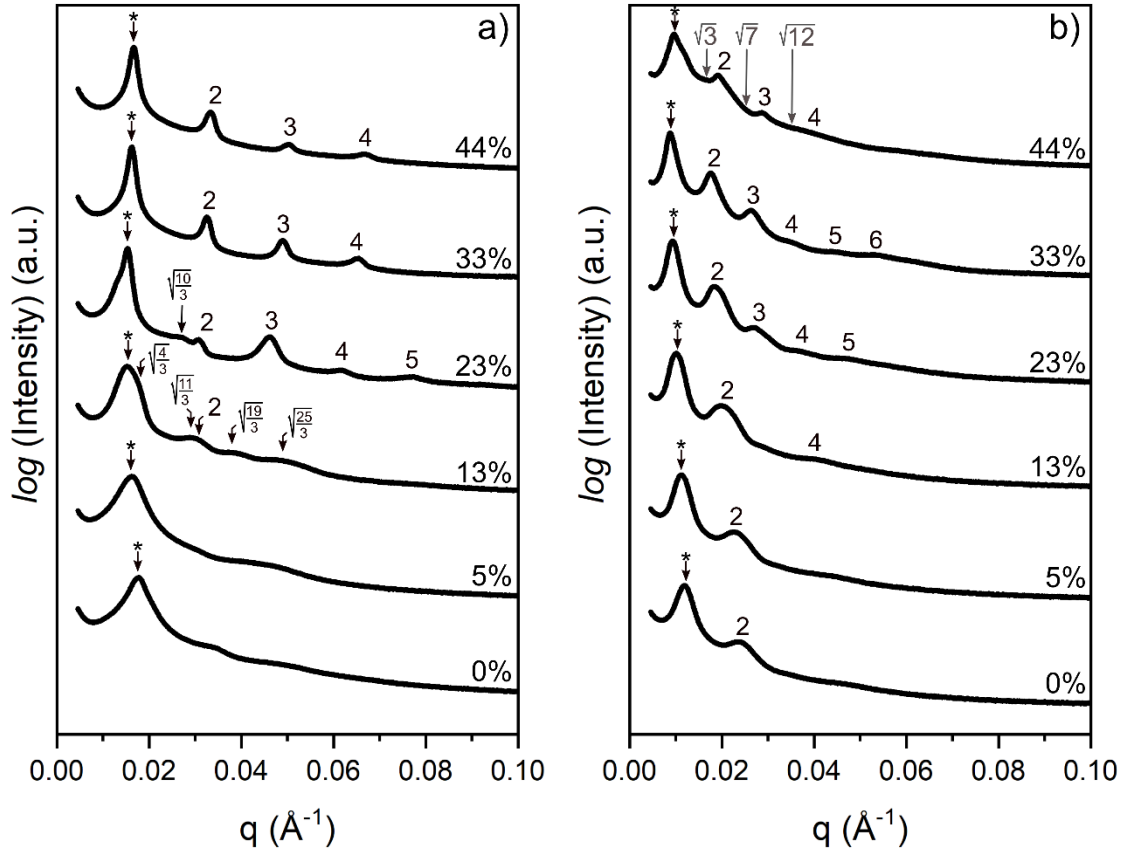
Figure 5. SAXS profiles of MAM (a) M53 and (b) M52 BCPs with different ionic liquid (IL) content φ_{IL} indicated on the graphs 0%, 5%, 13%, 23%, 33%, and 44%.

In **Figure 6**, the superposition of the SAXS 1D profiles of MAM M53 with 18 wt%, 23 wt%, and 28 wt% of IL is presented. This profile of the MAM M53 with 18 wt% of IL shows diffraction peaks at $\sqrt{(10/3)}q^*$, $\sqrt{(19/3)}q^*$, and $3q^*$, which mainly confirms the presence of a gyroid morphology. The SAXS pattern of MAM M53 with 28 wt% IL confirms the well-ordered lamellar morphology by the appearance of numerous higher order peaks at $2q^*$, $3q^*$, and $4q^*$. However, at intermediate φ_{IL} (23 wt%), a mixed pattern between those of the 18 wt% and 28 wt% can be observed with the gyroid scattering peaks ($\sqrt{(10/3)}q^*$, $\sqrt{(19/3)}q^*$) being gradually replaced by that of the lamellar morphology, confirming the transition between the gyroid and the lamellar morphology. As previously mentioned, AFM confirmed the coexistence

of two different morphologies, namely the lamellar and the gyroid morphologies revealed respectively by lines and 4-fold symmetry in the sample MAM M53 with 18 wt% of IL. The 4-fold symmetry could be a sign of gyroid structure for MAM M53 as it was confirmed with high-symmetry projections showing p6mm, p4mm, and c2mm symmetries observed by TEM and SEM in the literature, especially p4mm with <100> projection direction.[64,65] This is also confirmed by SAXS scattering patterns, where peaks corresponding to the lamellar morphology and to the gyroid morphologies. In the literature, it is common to obtain the coexisted morphologies with curved interface for polydisperse BCP.[61,63,64] Joan M. Widin et al. found that the coupling of block polydispersity, the consequent composition polydispersity, and ABA triblock chain topology could frustrate long-range ordering to yield a disordered bicontinuous structure that remains microphase-separated at very low values of χN as compared with corresponding monodisperse ABA triblocks.[61,63] Comparing with morphological characterization of ABA type triblock copolymers with gyroid morphology from the literature,[64] we confirmed the coexistence of lamellar and gyroid morphology for MAM M53 18 and 23 wt% IL.
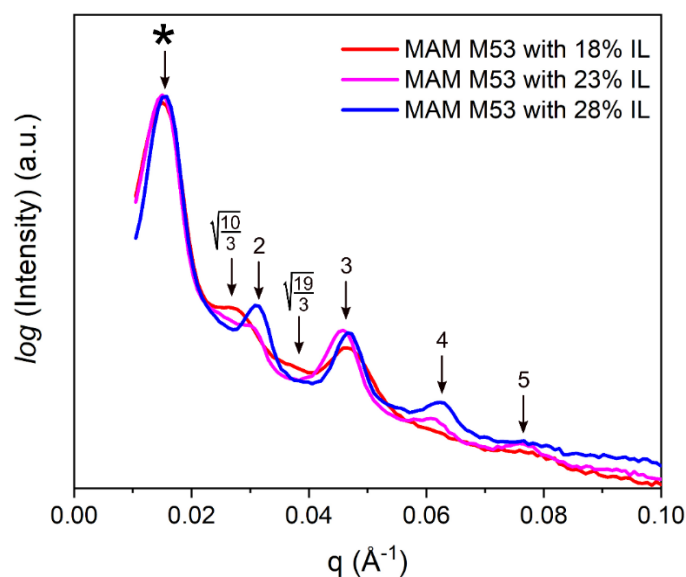
Figure 6. SAXS profiles of MAM M53 BCP with different ionic liquid (IL) content φ_{IL} 18%, 23%, and 28%.

It is noteworthy that the shape and the position of the first scattering peak ($q*$) of each curve appear to change as the IL concentration increases. Broader peaks at low IL concentrations and thinner peaks as the concentration increases were detected, which can confirm the presence of well-ordered morphology at the high concentration of IL in films. **Figure 7** shows the evolution of the full-width-half-maximum (FWHM) and the position of the primary peak $q*$ in each SAXS profile with the weight fraction φ_{IL} of IL.[66,67] In **Figure 7a**, the point of inflection on the FWHM profile was interpreted as the DOT (disorder-to-order transition) point and, in the case of MAM M53, takes place around 20 wt% of IL, which is in good agreement with the AFM observations. This effect is well pronounced for the M53 BCP with a transition from non-ordered state to a nanostructured morphology. For M52, the DOT is not detected, as only a smooth decrease without any abrupt inflection point can be observed. Since MAM M52 without IL already shows a lamellar morphology, no lyotropic DOT can be detected. Adding IL to this system only improves the interfaces between the two phases, leading to a slight and monotonous decrease of the FWMH.[33,53,66]

Figure 7b shows the evolution of the primary peak position $q*$. First, it can be seen that, for both BCP, peaks shift to lower q with increasing the IL content, indicating an increase in the size of the scattering objects. This can be attributed to one of the phases (PMMA, according to the DSC thermograms) being swollen by the IL. As the IL content is getting higher, the PMMA phase swells to the point that order-to-order transitions (OOT) can be detected. For M53, two changes of slopes (at 13 wt% and 23 wt%) can be noticed and correspond to the DIS $\rightarrow$ GYR and to the GYR $\rightarrow$ LAM transitions. For M52, the change of slope is detected at 33 wt% and corresponds to the LAM $\rightarrow$ CYL transition. Lai et al. also reported small shifts during the evolution of $q*$ upon heating, which indicated the OOT temperatures.[66] It is noteworthy that

similar results can be observed upon increasing the IL content. Carefully examining the SAXS patterns of MAM M53 and M52 polymers confirmed the disorder-to-order and order-to-order lyotropic transitions with different concentrations of IL in the BCP. This study validated once more the similarities of behavior of IL containing BCPs and lithium salt doped analogues.[33,53,67–69]
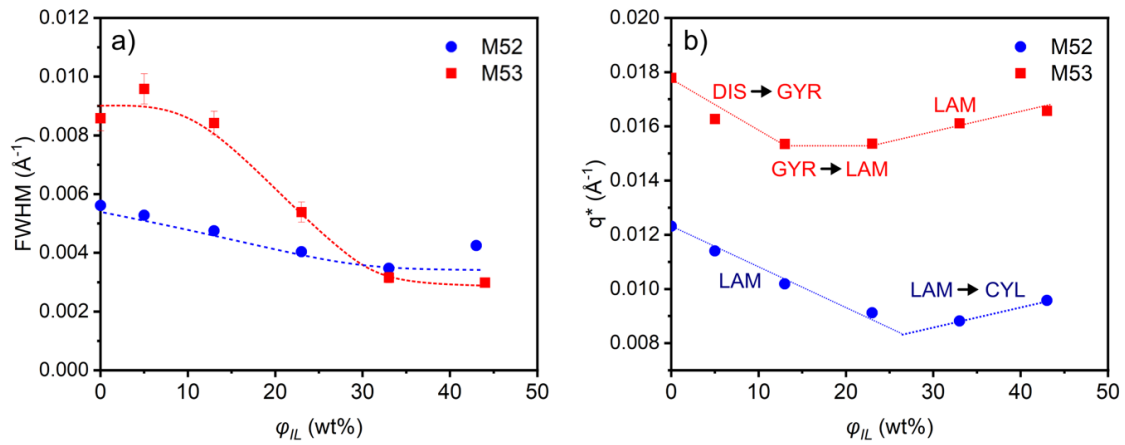

Figure 7. (a) FWHM of the primary scattering peak (q*) and (b) the primary peak position (q*) observed in the 1D SAXS profiles for MAM M53 and M52 block copolymer measured for varying ionic liquid (IL) weight concentrations φ_{IL}: from 0% to 44%. Lines are guides to the eye.

Bennett et al. reported that the selectivity of IL in polymers could be quantified by a detailed investigation of the variations of the lamellar domain spacing, *d*, with the polymer concentration.[32,33] They confirmed that for lamellar morphology, *d* is known to exhibit a power-law relationship in respect to the polymer volume fraction when a solvent that is selective for one of the blocks is added:[13,66]

$$d \sim \phi_P^{\alpha} = \phi_{IL}^{-\alpha} \qquad \text{(Eq. 2)}$$

where α is a measure of the solvent selectivity and φ_P is the polymer volume fraction. *d* was calculated using the position of the primary scattering peak of the SAXS 1D profiles for the lamellar morphologies *q** (Equation 3):

$$d = \frac{2\pi}{q*} \qquad \text{(Eq. 3)}$$

In this relationship, positive values of α correspond to a nonselective solvent which is good for both blocks and negative values of α fit with the presence of a strongly selective solvent.[13,30,47,66,70]
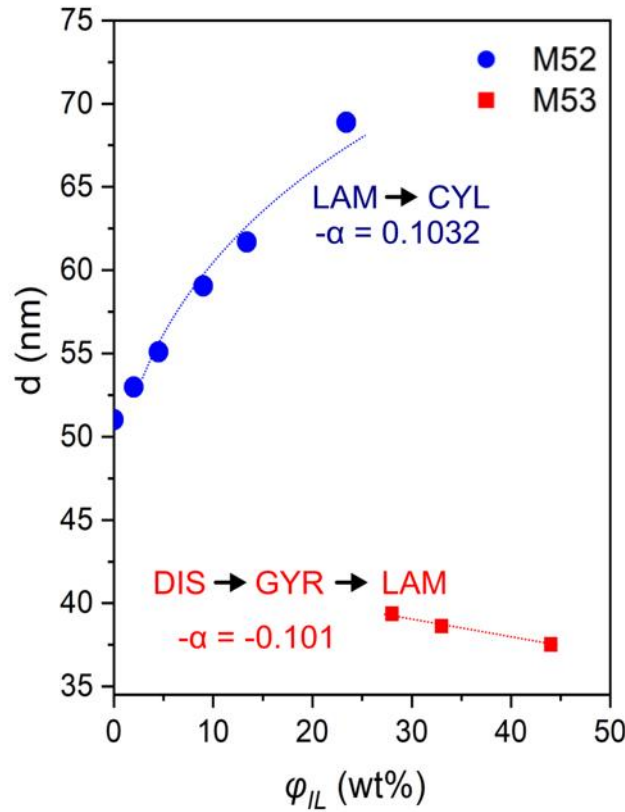

Figure 8. Domain spacing *d* of lamellar morphology for MAM M53 (red) and M52 (blue) block copolymer measured by SAXS for varying ionic liquid (IL) weight concentrations. Fitting curves correspond to power law fit for *α*.

Figure 8 shows the plots of the lamellar domain spacing *d* measured with the position of the primary scattering peak of the SAXS 1D profiles for samples with a lamellar morphology, as a function of φ_{IL}. As we focus on the evolution of the lamellar domain spacing *d* with φ_{IL} instead of φ_P, in our case, positive values of *α* represent selective solvent and negative values of *α* match with non-selective solvent compared to the literature (see Equation 2).[20,21,36,53,66]

The value of α for MAM 52 is -0.103±0.017, which is broadly consistent with the previous

studies from the literature on the blends of BCPs with strongly selective solvents and ILs where

values range between 0 and -3.16 (as a function of φ_P).[13,30,47,66,70] In the case of MAM M52,

this value is negative, which can be interpreted as a selective incorporation of IL to the PMMA

block. As the volume of the PMMA phase increases, the domain spacing of the lamellar
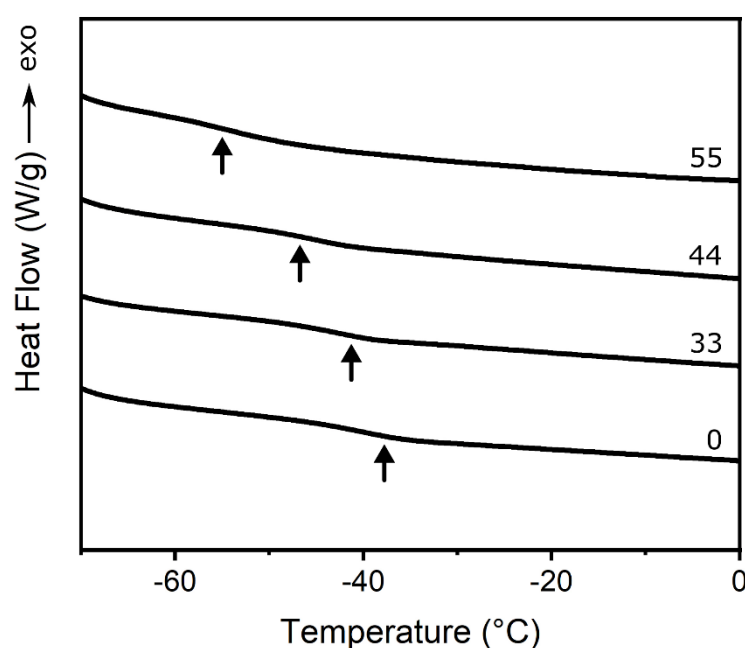
morphology increases until a LAM → CYL OOT occurs.

Figure 9. DSC curves for MAM M53 block copolymer blended with ionic liquid (IL) over different weight concentrations (φ_{IL}): 0%, 33%, 44%, and 55%. The black arrows indicate the T_gs of the PBuA block.

However, on **Figure 8**, a positive value of α was observed for MAM M53 (0.101±0.005)

shows that IL became gradually non-selective for MAM M53 blocks at higher IL concentration.

This result is in good agreement with Figure 1 where the small shifting of T_g of the PBuA block

was observed at high concentration of IL (starting from 33 wt% of IL). A film of MAM M53

with 55 wt% of IL was analyzed by DSC to confirm this tendency and has been compared with

the analyses for MAM M53 without IL and with 33 wt% and 44 wt% on **Figure 9**. The decrease

in the T_g of PBuA confirmed the non-selective miscibility of IL in the two blocks for high IL concentrated MAM M53 polymer mixtures, which is in line with our expectations. As the polarity difference between PMMA and PBuA is not very important, for high IL concentrated mixtures, the non-selective blending of polymer and IL can be observed. In the literature, it was shown, for low molar masses, the value of α decreases as a function of N, and then plateaus at high molar masses, reaching a value of -1.7 for PS-PMMA copolymers. Maximum values of α close to -0.5 were obtained for very low N (100, corresponding to Mw = 10 kg/mol).[32,33] In our case, the values of α are much lower compared to the results from the literature, due to the low polarity difference between the two blocks, even though ILs are reported to be highly selective. Since α is close to 0, a change in the molar mass leads to a sign shifting for α. For specific applications, this might be interesting to use such BCP blends if gyroid morphologies, which are difficult to obtain at higher molecular weight, are targeted.

Conclusions

In conclusion, we studied the effect of ionic liquid addition on the self-assembly process of commercially available poly(methyl methacrylate-*b*-butyl acrylate-*b*-methyl methacrylate) (MAM) triblock copolymers with an elastomeric central block and rigid end blocks. Two different compositions (MAM M52 and MAM M53) of the same copolymer were tested with and without ionic liquids (ILs) to study the effect of IL on the structuration of non-ordered BCPs, the improvement of existed nanostructured morphologies, and the order-order transition. The initial morphology of MAM M52 and MAM M53 films without ionic liquid is lamellar and disordered nanostructures, respectively. Our goal was to understand the IL effect on the self-assembly of MAM type BCP with low χ parameter and to observe the limit of IL content that may be attained in this configuration. Distortions of the phase diagram has been observed as a function of IL concentration in the studied block copolymers. The addition of ILs on MAM

M52 BCP resulted in more homogeneous and organized lamellae reaching a saturation at the concentration of 33 wt%. In the case of the MAM M53 BCP, it induced a lyotropic DOT from non-specific morphology to coexisting gyroid and lamellar morphologies with IL saturation for φ_{IL} between 13 and 23 wt% even for high molecular weight copolymer, due to the low χ parameter. In addition, for MAM M53, well-ordered morphology was obtained after the solvent casting of the film by adding ILs without any thermal annealing from initially non-ordered polymer. To our knowledge, in most of the studies, researchers applied a solvent vapor annealing step or thermal heating after film casting to increase the mobility of polymer chains to obtain targeted nanostructure. The perspective of this work for soft actuator applications will focus on the gyroid morphology with other types of IL, which will overcome the challenges associated with optimizing the concentration of ion containing blocks in these systems, in order to achieve high moduli systems by having gyroid nanostructure with large domains in order to limit the sacrifices to ionic conductivity.

Acknowledgments

References

1. Bates, C. M., Maher, M. J., Janes, D. W., Ellison, C. J. & Willson, C. G. Block Copolymer Lithography. *Macromolecules* **47**, 2–12 (2014).

2. Young, W.-S., Kuan, W.-F. & Epps, T. H. Block copolymer electrolytes for rechargeable lithium batteries. *J. Polym. Sci. Part B Polym. Phys.* **52**, 1–16 (2014).

3. Segalman, R. A., McCulloch, B., Kirmayer, S. & Urban, J. J. Block Copolymers for Organic Optoelectronics. *Macromolecules* **42**, 9205–9216 (2009).

4. Black, C. T. *et al.* Polymer self assembly in semiconductor microelectronics. *IBM J. Res. Dev.* **51**, 605–633 (2007).

5. Yang, G. G. *et al.* Block Copolymer Nanopatterning for Nonsemiconductor Device Applications. *ACS Appl. Mater. Interfaces* **14**, 12011–12037 (2022).

6. Gu, X., Gunkel, I. & Russell, T. P. Pattern transfer using block copolymers. *Philos. Trans. R. Soc. Math. Phys. Eng. Sci.* **371**, 20120306 (2013).

7. Ahn, S. *et al.* Gyroid Structures at Highly Asymmetric Volume Fractions by Blending of ABC Triblock Terpolymer and AB Diblock Copolymer. *Macromolecules* **50**, 9008–9014 (2017).

8. Gottlieb, E. R., Guliyeva, A. & Epps, T. H. From Lab to Fab: Enabling Enhanced Control of Block Polymer Thin-Film Nanostructures. *ACS Appl. Polym. Mater.* **3**, 4288–4303 (2021).

9. Epps, III, T. H. & O'Reilly, R. K. Block copolymers: controlling nanostructure to generate functional materials – synthesis, characterization, and engineering. *Chem. Sci.* **7**, 1674–1689 (2016).

10. Deepthi, K., Stamm, M. & Gowd, E. B. Factors influencing the formation of block copolymer-based supramolecular assemblies in bulk and thin films. *Mater. Today Commun.* **24**, 101147 (2020).

11. Gowd, E. B., Koga, T., Endoh, M. K., Kumar, K. & Stamm, M. Pathways of cylindrical orientations in PS-b-P4VP diblock copolymer thin films upon solvent vapor annealing. *Soft Matter* **10**, 7753–7761 (2014).

12. Lodge, T. P., Pudil, B. & Hanley, K. J. The Full Phase Behavior for Block Copolymers in Solvents of Varying Selectivity. *Macromolecules* **35**, 4707–4717 (2002).

13. Hanley, K. J., Lodge, T. P. & Huang, C.-I. Phase Behavior of a Block Copolymer in Solvents of Varying Selectivity. *Macromolecules* **33**, 5918–5931 (2000).

14. Roland, S. *et al.* Solvent Influence on Thickness, Composition, and Morphology Variation with Dip-Coating Rate in Supramolecular PS-b-P4VP Thin Films. *Macromolecules* **48**, 4823–4834 (2015).

15. Roland, S., Pellerin, C., Bazuin, C. G. & Prud'homme, R. E. Evolution of Small Molecule Content and Morphology with Dip-Coating Rate in Supramolecular PS–P4VP Thin Films. *Macromolecules* **45**, 7964–7972 (2012).

16. Roland, S., Prud'homme, R. E. & Bazuin, C. G. Morphology, Thickness, and Composition Evolution in Supramolecular Block Copolymer Films over a Wide Range of Dip-Coating Rates. *ACS Macro Lett.* **1**, 973–976 (2012).

17. Vukovic, I. *et al.* Double Gyroid Network Morphology in Supramolecular Diblock Copolymer Complexes. *Macromolecules* **45**, 3503–3512 (2012).

18. Vukovic, I. *et al.* Supramolecular Route to Well-Ordered Metal Nanofoams. *ACS Nano* **5**, 6339–6348 (2011).

19. Böhme, M., Kuila, B., Schlörb, H., Nandan, B. & Stamm, M. Thin films of block copolymer supramolecular assemblies: Microphase separation and nanofabrication. *Phys. Status Solidi B* **247**, 2458–2469 (2010).

20. Nandan, B., Kuila, B. K. & Stamm, M. Supramolecular assemblies of block copolymers as templates for fabrication of nanomaterials. *Eur. Polym. J.* **47**, 584–599 (2011).

21. Nandan, B., Vyas, M. K., Böhme, M. & Stamm, M. Composition-Dependent Morphological Transitions and Pathways in Switching of Fine Structure in Thin Films of Block Copolymer Supramolecular Assemblies. *Macromolecules* **43**, 2463–2473 (2010).

22. Arias-Zapata, J. *et al.* Ultrafast Assembly of PS-PDMS Block Copolymers on 300 mm Wafers by Blending with Plasticizers. *Adv. Funct. Mater.* **26**, 5690–5700 (2016).

23. Forsyth, S. A., Pringle, J. M. & MacFarlane, D. R. Ionic Liquids—An Overview. *Aust. J. Chem.* **57**, 113–119 (2004).

24. Gordon, C. M. *et al.* Synthesis and Purification. in *Ionic Liquids in Synthesis* 7–55 (John Wiley & Sons, Ltd, 2007).

25. Welton, T. Room-Temperature Ionic Liquids. Solvents for Synthesis and Catalysis. *Chem. Rev.* **99**, 2071–2084 (1999).

26. McFarlane, D. R., Sun, J., Golding, J., Meakin, P. & Forsyth, M. High conductivity molten salts based on the imide ion. *Electrochimica Acta* **45**, 1271–1278 (2000).

27. Ueki, T. & Watanabe, M. Macromolecules in Ionic Liquids: Progress, Challenges, and Opportunities. *Macromolecules* **41**, 3739–3749 (2008).

28. Ueki, T. & Watanabe, M. Polymers in Ionic Liquids: Dawn of Neoteric Solvents and Innovative Materials. *Bull. Chem. Soc. Jpn.* **85**, 33–50 (2012).

29. Tamate, R., Hashimoto, K., Ueki, T. & Watanabe, M. Block copolymer self-assembly in ionic liquids. *Phys. Chem. Chem. Phys.* **20**, 25123–25139 (2018).

30. Simone, P. M. & Lodge, T. P. Phase Behavior and Ionic Conductivity of Concentrated Solutions of Polystyrene-Poly(ethylene oxide) Diblock Copolymers in an Ionic Liquid. *ACS Appl. Mater. Interfaces* **1**, 2812–2820 (2009).

31. Bennett, T. M. *et al.* Can ionic liquid additives be used to extend the scope of poly(styrene)-block-poly(methyl methacrylate) for directed self-assembly? *J. MicroNanolithography MEMS MOEMS* **13**, 031304 (2014).

32. Bennett, T. M., Jack, K. S., Thurecht, K. J. & Blakey, I. Perturbation of the Experimental Phase Diagram of a Diblock Copolymer by Blending with an Ionic Liquid. *Macromolecules* **49**, 205–214 (2016).

33. Bennett, T. M., Chambers, L. C., Thurecht, K. J., Jack, K. S. & Blakey, I. Dependence of Block Copolymer Domain Spacing and Morphology on the Cation Structure of Ionic Liquid Additives. *Macromolecules* **51**, 8979–8986 (2018).

34. Kim, O., Kim, S. J. & Park, M. J. Low-voltage-driven soft actuators. *Chem. Commun.* **54**, 4895–4904 (2018).

35. Kim, O., Kim, S. Y., Park, B., Hwang, W. & Park, M. J. Factors Affecting Electromechanical Properties of Ionic Polymer Actuators Based on Ionic Liquid-Containing Sulfonated Block Copolymers. *Macromolecules* **47**, 4357–4368 (2014).

36. Virgili, J. M., Hexemer, A., Pople, J. A., Balsara, N. P. & Segalman, R. A. Phase Behavior of Polystyrene- *block* -poly(2-vinylpyridine) Copolymers in a Selective Ionic Liquid Solvent. *Macromolecules* **42**, 4604–4613 (2009).

37. Virgili, J. M., Nedoma, A. J., Segalman, R. A. & Balsara, N. P. Ionic Liquid Distribution in Ordered Block Copolymer Solutions. *Macromolecules* **43**, 3750–3756 (2010).

38. Virgili, J. M., Hoarfrost, M. L. & Segalman, R. A. Effect of an Ionic Liquid Solvent on the Phase Behavior of Block Copolymers. *Macromolecules* **43**, 5417–5423 (2010).

39. Zhang, S., Lee, K. H., Frisbie, C. D. & Lodge, T. P. Ionic Conductivity, Capacitance, and Viscoelastic Properties of Block Copolymer-Based Ion Gels. *Macromolecules* **44**, 940–949 (2011).

40. Chen, X. *et al.* Ionic Liquids as Additives to Polystyrene- *Block* -Poly(Methyl Methacrylate) Enabling Directed Self-Assembly of Patterns with Sub-10 nm Features. *ACS Appl. Mater. Interfaces* **10**, 16747–16759 (2018).

41. Ye, Y.-S., Rick, J. & Hwang, B.-J. Ionic liquid polymer electrolytes. *J. Mater. Chem. A* **1**, 2719–2743 (2013).

42. Kim, S. J., Kim, O. & Park, M. J. True Low-Power Self-Locking Soft Actuators. *Adv. Mater.* **30**, 1706547 (2018).

43. Kim, O., Kim, H., Choi, U. H. & Park, M. J. One-volt-driven superfast polymer actuators based on single-ion conductors. *Nat. Commun.* **7**, 13576 (2016).

44. Noro, A. *et al.* Photonic Block Copolymer Films Swollen with an Ionic Liquid. *Macromolecules* **47**, 4103–4109 (2014).

45. Imaizumi, S., Kokubo, H. & Watanabe, M. Polymer Actuators Using Ion-Gel Electrolytes Prepared by Self-Assembly of ABA-Triblock Copolymers. *Macromolecules* **45**, 401–409 (2012).

46. Hashimoto, K. *et al.* Transport and Mechanical Properties of ABA-type Triblock Copolymer Ion Gels Correlated with Their Microstructures. *Macromolecules* **52**, 8430–8439 (2019).

47. Simone, P. M. & Lodge, T. P. Lyotropic Phase Behavior of Polybutadiene-Poly(ethylene oxide) Diblock Copolymers in Ionic Liquids. *Macromolecules* **41**, 1753–1759 (2008).

48. Ruzette, A.-V. *et al.* Molecular Disorder and Mesoscopic Order in Polydisperse Acrylic Block Copolymers Prepared by Controlled Radical Polymerization. *Macromolecules* **39**, 5804–5814 (2006).

49. Sriprom, W., James, M., Perrier, S. & Neto, C. Ordered Microphase Separation in Thin Films of PMMA–PBA Synthesized by RAFT: Effect of Block Polydispersity. *Macromolecules* **42**, 3138–3146 (2009).

50. Russell, T. P., Hjelm, R. P. & Seeger, P. A. Temperature dependence of the interaction parameter of polystyrene and poly(methyl methacrylate). *Macromolecules* **23**, 890–893 (1990).

51. Sawyer, L. C., Grubb, D. T. & Meyers, G. F. *Polymer Microscopy*. (Springer New York, 2008).

52. Susan, Md. A. B. H., Kaneko, T., Noda, A. & Watanabe, M. Ion Gels Prepared by in Situ Radical Polymerization of Vinyl Monomers in an Ionic Liquid and Their Characterization as Polymer Electrolytes. *J. Am. Chem. Soc.* **127**, 4976–4983 (2005).

53. Nakamura, I., Balsara, N. P. & Wang, Z.-G. First-Order Disordered-to-Lamellar Phase Transition in Lithium Salt-Doped Block Copolymers. *ACS Macro Lett.* **2**, 478–481 (2013).

54. Thelen, J. L. *et al.* Phase Behavior of a Block Copolymer/Salt Mixture through the Order-to-Disorder Transition. *Macromolecules* **47**, 2666–2673 (2014).

55. Lynd, N. A., Meuler, A. J. & Hillmyer, M. A. Polydispersity and block copolymer self-assembly. *Prog. Polym. Sci.* **33**, 875–893 (2008).

56. Cooke, D. M. & Shi, A.-C. Effects of Polydispersity on Phase Behavior of Diblock Copolymers. *Macromolecules* **39**, 6661–6671 (2006).

57. Widin, J. M. *et al.* Bulk and Thin Film Morphological Behavior of Broad Dispersity Poly(styrene- *b*- methyl methacrylate) Diblock Copolymers. *Macromolecules* **46**, 4472–4480 (2013).

58. Burger, C., Ruland, W. & Semenov, A. N. Polydispersity effects on the microphase-separation transition in block copolymers. *Macromolecules* **23**, 3339–3346 (1990).

59. Sides, S. W. & Fredrickson, G. H. Continuous polydispersity in a self-consistent field theory for diblock copolymers. *J. Chem. Phys.* **121**, 4974–4986 (2004).

60. Matsen, M. W. Comparison of A-block polydispersity effects on BAB triblock and AB diblock copolymer melts. *Eur. Phys. J. E* **36**, 44 (2013).

61. Widin, J. M., Schmitt, A. K., Im, K., Schmitt, A. L. & Mahanthappa, M. K. Polydispersity-Induced Stabilization of a Disordered Bicontinuous Morphology in ABA Triblock Copolymers. *Macromolecules* **43**, 7913–7915 (2010).

62. Schmitt, A. L. & Mahanthappa, M. K. Polydispersity-driven shift in the lamellar mesophase composition window of PEO-PB-PEO triblock copolymers. *Soft Matter* **8**, 2294–2303 (2012).

63. Widin, J. M., Schmitt, A. K., Schmitt, A. L., Im, K. & Mahanthappa, M. K. Unexpected Consequences of Block Polydispersity on the Self-Assembly of ABA Triblock Copolymers. *J. Am. Chem. Soc.* **134**, 3834–3844 (2012).

64. Avgeropoulos, A., Dair, B. J., Hadjichristidis, N. & Thomas, E. L. Tricontinuous Double Gyroid Cubic Phase in Triblock Copolymers of the ABA Type. *Macromolecules* **30**, 5634–5642 (1997).

65. Dehmel, R. *et al.* Optical Imaging of Large Gyroid Grains in Block Copolymer Templates by Confined Crystallization. *Macromolecules* **50**, 6255–6262 (2017).

66. Lai, C., Russel, W. B. & Register, R. A. Phase Behavior of Styrene-Isoprene Diblock Copolymers in Strongly Selective Solvents. *Macromolecules* **35**, 841–849 (2002).

67. Wolff, T., Burger, C. & Ruland, W. Synchrotron SAXS study of the microphase separation transition in diblock copolymers. *Macromolecules* **26**, 1707–1711 (1993).

68. Nakamura, I. Microphase Separation of Ionic Liquid-Containing Diblock Copolymers: Effects of Dielectric Inhomogeneity and Asymmetry in the Molecular Volumes and Interactions between the Cation and Anion. *Macromolecules* **53**, 3891–3899 (2020).

69. Nakamura, I. & Wang, Z.-G. Thermodynamics of Salt-Doped Block Copolymers. *ACS Macro Lett.* **3**, 708–711 (2014).

70. Hoarfrost, M. L. & Segalman, R. A. Ionic Conductivity of Nanostructured Block Copolymer/Ionic Liquid Membranes. *Macromolecules* **44**, 5281–5288 (2011).